IEEE Access
Multidisciplinary | Rapid Review | Open Access Journal

SPECIAL SECTION ON UNDERWATER WIRELESS COMMUNICATIONS AND NETWORKING

Received October 13, 2017, accepted December 4, 2017, date of publication January 8, 2018,
date of current version February 28, 2018.

Digital Object Identifier 10.1109/ACCESS.2018.2790478

Spread-Spectrum Techniques for Bio-Friendly Underwater Acoustic Communications

BENJAMIN SHERLOCK, (Member, IEEE), JEFFREY A. NEASHAM, AND CHARALAMPOS C. TSIMENIDIS, (Senior Member, IEEE)

School of Engineering, Newcastle University, Newcastle-upon-Tyne NE1 7RU, U.K.

Corresponding author: Benjamin Sherlock (benjamin.sherlock@ncl.ac.uk)

This work was supported in part by the U.K. Engineering and Physical Sciences Research Council through a Ph.D. Doctoral Training Account and in part by the USMART Project under Grant EP/P017975/1.

ABSTRACT This paper investigates techniques to mitigate the impact of acoustic communication signals on marine life, by minimizing source level and designing waveforms with characteristics proven to reduce animal discomfort in bioacoustics studies. High-ratio spread spectrum transmission is employed with bandwidth-time products exceeding 1000. Signaling is based on the families of near orthogonal pseudo-noise waveforms, generated by bandpass filtering of binary M-sequences. This enables reception of data, at very low SNR, over a radius many times greater than the radius of discomfort experienced by marine mammals. Computationally efficient receivers with novel synchronization structures needed to be developed to operate at very low SNR and with severe Doppler effects. Simulations show the proposed scheme is able to achieve 45 bit/s at −18-dB SNR and 140 bit/s at −12-dB SNR. Experimental system performance was assessed during realistic experiments in the North Sea, verifying performance over ranges up to 10 km with transmitted SL of <170 dB re 1 μPa at 1 m and with Doppler effects induced by relative motion exceeding 2 m/s. Conclusion: The system developed compares favorably, in terms of SNR performance and channel utilization, with previously reported work aimed at covert communication but offers reduced transmitter/receiver complexity and discomfort to animals. This paper offers a way forward to more bio-friendly acoustic modem devices for operation in regions with sensitive fauna and/or increasingly strict environmental controls.

INDEX TERMS Spread-spectrum, underwater acoustic modem, low-power, low-received-SNR, M-OCK, bio-friendly.

I. INTRODUCTION

Underwater acoustic modems play an increasingly important role in underwater sensor networks and the control/tracking of underwater vehicles. However, relatively little research has been dedicated to the impact of their acoustic emissions and how this may be reduced. As usage becomes more widespread in the future, it seems inevitable that acoustic modem deployments will come under more scrutiny from environmental groups and regulatory bodies.

Anthropogenic noise has been shown to have negative consequences on marine life ranging from injury and hearing loss to causing behavioural effects. These were conceptualised in a model for categorising the effect of noise on marine mammals devised by Richardson *et al*. in 1995 [1] and also included in the OSPAR report on impacts of anthropogenic underwater sound [2]. The Theoretical Zones of Noise Influence, as shown in Fig. 1, consist of four bands with the greatest sound energy and hence the greatest severity of impact shown at the centre. The degrees of influence are: 1) Hearing loss, discomfort, injury; 2) Response; 3) Masking; and 4) Detection/Audible.

Injury of the auditory system due to exposure to excessive sound can result in Permanent Threshold Shift (PTS) or Temporary Threshold Shift (TTS). Studies by Lucke *et al*. suggested that harbour porpoises may have the lowest TTS thresholds of any cetacean species tested at the point of publication in 2009. At 4 kHz they showed TTS at a sound pressure level of 199.7 dB_{pk-pk} re 1μPa and a sound exposure level of 164.3dB re 1μPa^2-s. However, the animal also showed behavioural reactions at sound pressure levels of 174 dB_{pk-pk} re 1μPa and sound exposure level of 145dB re 1μPa^2-s [3].

Behavioural studies by Kastelein *et al*. have shown the effect of acoustic data transmissions around 12 kHz on Harbour Porpoises (Phocoena phocoena) [4]. Experiments were

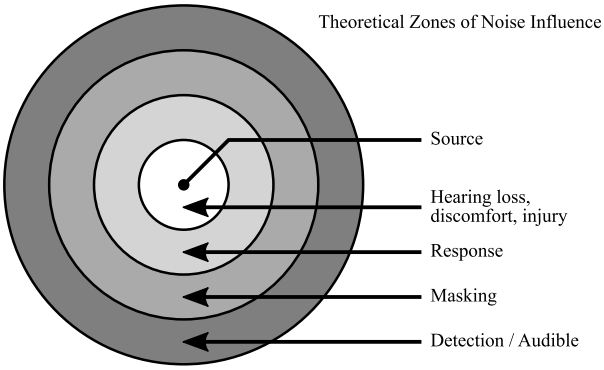

FIGURE 1. Theoretical zones of noise influence. originally by Richardson *et al.* [1].

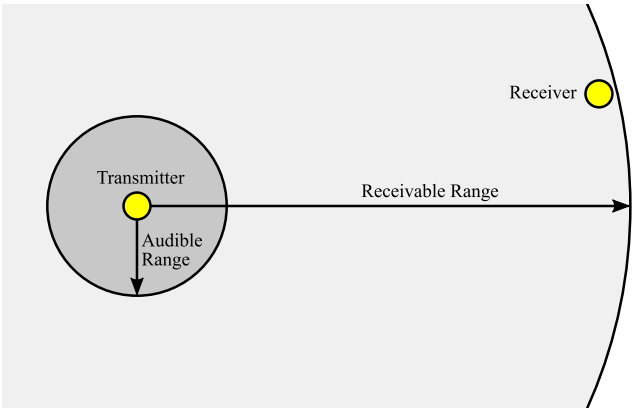

FIGURE 2. Audible-receivable ranges. Aim is to maximise the receivable range whilst reducing audible range.

carried out with two captive harbour porpoises, with four acoustic signal types tested: swept FM (chirps), DSSS, Frequency Sweep (1 s linear sweep between 10 kHz to 14 kHz for reference with previous experiments), and modulated FSK. Based on spectrograms for the four signals, the bandwidth for modulated FSK is 10 kHz to 13 kHz whereas the DSSS is 10 kHz to 18 kHz. The results were used to calculate the estimated radius of discomfort zone for each sound type based on a given source level (SL). For a source level of 170dB re 1μPa @ 1m, the estimated radius of discomfort zones were 6.3km for Chirp, 3.1km for DSSS, 5.6km for frequency sweep, and 1.26km for modulated FSK. The sound type of modulated FSK has zero gap between packets so appears as a continuous sound, whereas the DSSS sound occurs in 1.0 s blocks with 0.7 s intervals. Kastelein *et al.* previously determined that on-off switching sounds affect harbour porpoises [5]. Chirp sounds also have been shown to affect harbour porpoises [6]. From this it can be determined that continuous broadband noise-like signals have less impact than chirps and impulsive or on-off switching sounds.

Acoustic deterrent devices (ADD) are known to emit similar power levels and frequencies to those used in acoustic modems, along with modulation of amplitude and frequency in random bursts. Such devices have been proven to drive away seals and porpoises. For example, dolphin deterrents can have a SL of 175dB re 1μPa @ 1m at 40 kHz and seal deterrents a SL of 189dB re 1μPa @ 1m. Typical commercially available acoustic modems typically have SL up to and beyond 190dB re 1μPa @ 1m at frequencies of between 8 kHz and 40 kHz.

In order to minimise the potential environmental impact of acoustic data transmission there is a need, firstly, to reduce the transmitter acoustic power such that there is no zone that results in injury. Secondly, through signal and receiver design, the ratio between receivable range and audible range in Fig. 2 should be increased to limit the potential impact on marine mammals through behavioural responses or by masking marine mammal communication/echolocation signals.

Based on the research by Lucke *et al*. the transmitter power should limit the SPL to less than 174dB re 1μPa in the vicinity of the transmitter [3].

The work by Kastelein *et al*. also shows that the signal should be long-duration and noise-like rather than tonal, chirp or burst transmissions in order to minimise behavioural response [4]–[6].

Many systems targeting low-received-SNR are typically for the purposes of covert acoustic communications [7]–[11]. Signals are often described in terms of low probability of detection (LPD), and low probability of interception (LPI). High-ratio spread spectrum techniques are generally applied so that signals buried below the background noise can be recovered via the processing gain of the de-spreading process. This inevitably leads to a large reduction in data rate (bandwidth efficiency) but there are many underwater networking and positioning applications where data rates of less than 100 bit/s are adequate.

A three year European project "UUV - Covert Acoustic Communications (UCAC)" (Project RTP 110.060) explored covert communication schemes and channel conditions in littoral environments. Acoustic channel conditions were recorded and measured using probe signals, with a simulator subsequently produced [12], [13]. A number of modulation schemes, with constraints on bandwidth (3.5 kHz) and data rate (4.2 bit/s and 75 bit/s) with $^1/_3$-rate turbo code, were designed and tested using a simulator [12], [13] and in sea trials [14]–[21].

The DSSS with turbo equalization achieved performances of 4 bit/s at -14dB at a range of 52km. For data rate of 75 bit/s the performance was -6.5dB. All with a bandwidth of 3.5 kHz [19]. The channel capacity at -14dB is 197.12 bit/s indicating a channel utilisation of 2.03% for the lower data rate. The channel capacity at -6.5dB is 1020.08 bit/s indicating a channel utilisation of 7.35% for the higher data rate.

The multiband OFDM achieved performances of 4.2 bit/s at -17dB at a range of 52km. For data rate of 78 bit/s the performance was -8dB. The performance of the lower data rate packets were ultimately limited by the ability to successfully synchronise. The modulation scheme with coding in simulation showed a potential performance of BER 10^{-4} at SNR of -20dB. The bandwidth is 3.6 kHz. [17], [18].

The channel capacity at −17dB is 102.61 bit/s indicating a channel utilisation of 4.09% for the lower data rate. The channel capacity at −8dB is 764.08 bit/s indicating a channel utilisation of 10.21% for the higher data rate.

The multicarrier spread spectrum scheme (MCSS) achieved performances of 75 bit/s at −12dB at ranges up to and including 52km. The bandwidth is 3.68 kHz [15], [16]. The channel capacity at −12dB is 324.84 bit/s indicating a channel utilisation of 23.09%. These schemes make use of complex receiver structures and computationally-intensive turbo decoders in order to achieve low-received-SNR communications at these data rates and SNR levels.

This paper explores a detailed investigation of an M-ary orthogonal transmission scheme, first proposed by Dimitrov *et al.* [22], and synchronisation and receiver structures to achieve low-received-SNR communications. The signal characteristics are well suited for reducing impact on marine mammals, with continuous transmission of a near-perfect white noise spectrum. Transmitter complexity is very low and receiver complexity is modest, with acceptable bit error rates achievable via relatively simple forward error correction codes such as Reed-Solomon.

The paper is organised into the following structure. The signal design is investigated in Section II. The receiver design for synchronisation and data demodulation is presented in Section III. Doppler compensation techniques in signal and receiver design are investigated in Section IV.

II. SIGNAL DESIGN

A well proven spread-spectrum communication technique in underwater acoustic channels utilises binary orthogonal LFM chirp signals (Chirp-BOK). Comparing LFM chirps and a bandlimited PN sequence of the same bandwidth, duration and energy it is clear to see that as the SNR decreases the PN sequence becomes harder to distinguish from background noise before the chirp as shown in Fig. 3. This illustrates why deterministic signals were found by Kastelein *et al*. to cause a larger radius of discomfort for marine mammals than random, noise like signals.

The binary orthogonal keying concept can be taken further by using sets of near-orthogonal PN codes that allow the modulation depth, M, and the spectral efficiency to be increased. We refer to this as M-ary orthogonal code keying (M-OCK). The "chips" of the PN codes may be modulated onto a carrier via BPSK. However in this work it is preferred to generate longer PN codes at a chip frequency of at least twice the highest frequency of the acoustic band and then bandpass filter to the required bandwidth. The signal is constructed from unique bandlimited PN codes that are M-ary mapped from the data as shown in Fig. 4. This generates a truer white noise spectrum which also has slightly improved correlation properties compared to BPSK modulated sequences [22]. In practical implementation this filtering can be provided by the acoustic transducer itself allowing a transmitter composed simply of the PN sequence generators (shift register) and a switching amplifier driving the transducer.

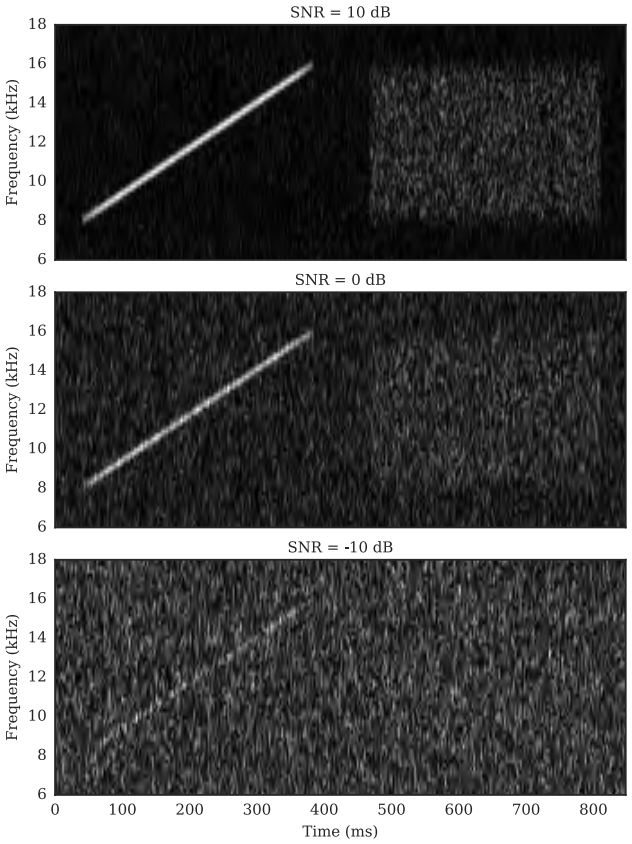

FIGURE 3. Waterfall plot (Frequency vs Time) of bandlimited PN vs linear chirp with varying AWGN noise.

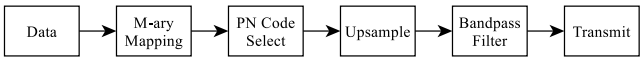

FIGURE 4. PN transmit block diagram. Data is m-ary mapped to unique PN codes which are upsampled then bandlimited prior to transmission.

Orthogonality of the modulation scheme implies that all messages are equiprobable a priori. Proakis provides the equation for maximum likelihood detection of such messages [23, eq. (4.1–11)] in (1). Where the a priori probabilities, $P_m = \frac{1}{M}$ for all $1 \leq m \leq M$, $\mathbf{r}$ is the received vector, $\mathbf{s}_m$ is the signal vector, $p(\mathbf{r}|\mathbf{s}_m)$ is the likelihood of message m.

$$\hat{m} = \underset{1 \leq m \leq M}{\arg\max}\, p(\mathbf{r}|\mathbf{s}_m) \tag{1}$$

Probability of symbol error and bit error for an m-ary orthogonal signaling scheme has been analysed by Proakis [23, Sec. 4.4-1] who provides the equations below. Where the probability of symbol error, P_e, can be solved for a given symbol energy, ϵ, noise, N_0, and number of possible orthogonal symbols, M, in (2). This can then be used to calculate the bit error, P_b, for a given number of data bits per symbol, k, where $M = 2^k$, in (4).

$$P_e = \frac{1}{\sqrt{2\pi}} \int_{-\infty}^{\infty} \left[1 - (1 - Q(x))^{M-1}\right] e^{-\frac{\left(x - \sqrt{\frac{2\epsilon}{N_0}}\right)^2}{2}} \mathrm{d}x \tag{2}$$

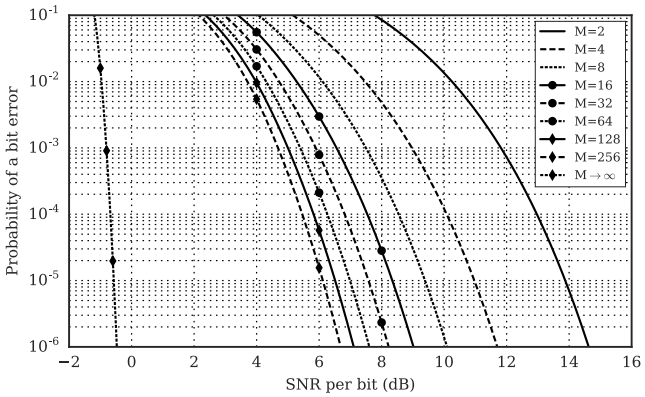

FIGURE 5. Upper bound BER vs ϵ_b/N_0 for various values of M for M-ary orthogonal signaling with values of M ranging from 2 to 256. For M→ ∞ the value used is $M = 2^{1000}$. Generated using the formula by Proakis [23, Sec. 4.4–1].

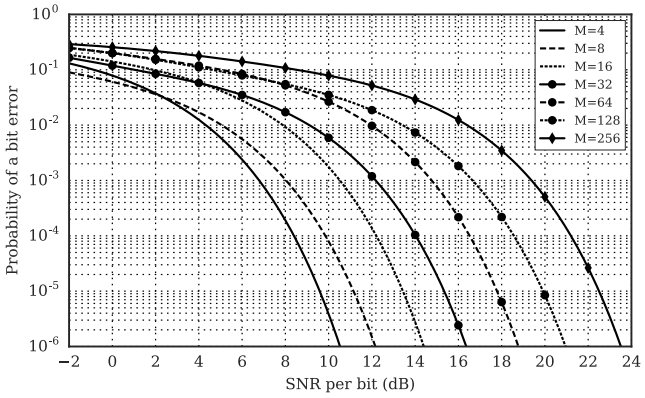

FIGURE 6. BER vs ϵ_b/N_0 for various values of M for M-ary quadrature amplitude modulation with values of M ranging from 4 to 256. Generated using approximation 2 by Yang and Hanzo [24].

Equation (2) has no known closed form, however an upper or union bound equation is provided by Proakis and Salehi [23] as shown in (3) Where $k = \log_2 M$ and $\frac{\epsilon_b}{N_0} > \ln 2 = 0.693 \approx -1.6\,dB$.

$$P_e \leqslant \begin{cases} e^{-\frac{k}{2}\left(\frac{\epsilon_b}{N_0} - 2\ln 2\right)}, & \dfrac{\epsilon_b}{N_0} > 4\ln 2 \\ 2e^{-k\left(\sqrt{\frac{\epsilon_b}{N_0}} - \sqrt{\ln 2}\right)^2}, & \ln 2 \leqslant \dfrac{\epsilon_b}{N_0} \leqslant 4\ln 2 \end{cases} \tag{3}$$

Taking the upper bound probability of symbol error the respective bit error is calculated using (4).

$$P_b = 2^{k-1}\frac{P_e}{2^k - 1} \tag{4}$$

As the modulation depth is increased, the energy-per-bit required to maintain a given bit error probability is decreased, as shown in Fig. 5.

In contrast, for other M-ary modulation schemes such as M-QAM, as the modulation depth increases, the bit error rate performance decreases as shown in Fig. 6.

Maximal length sequences (M-Sequences) are a form of pseudorandom-noise (PN) sequence, where a given order

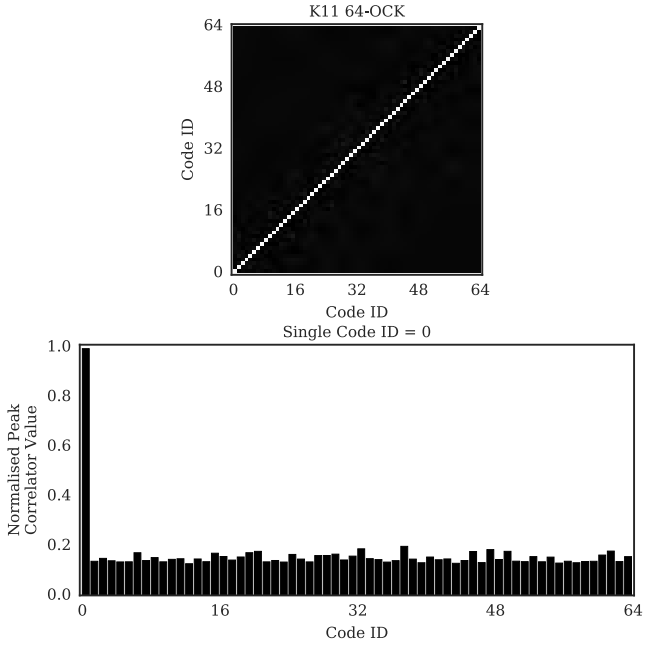

FIGURE 7. Cross correlation properties of bandlimited M-Sequence code set. $K = 11$, code set size = 64.

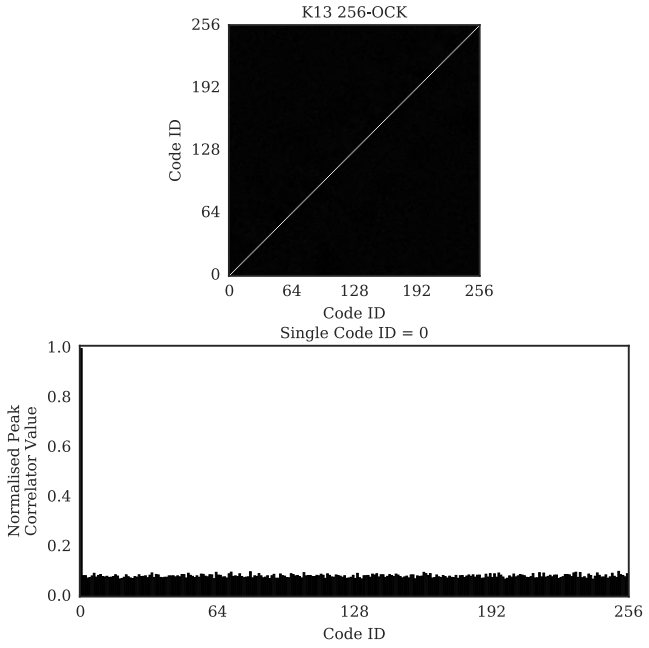

FIGURE 8. Cross correlation properties of bandlimited M-Sequence code set. $K = 13$, code set size = 256.

of K results in a unique sequence of length $N = 2^K - 1$, as covered in depth by Golomb [25], [26]. Tables of the auto- and cross-correlation properties have been produced by Proakis [23, Table 12.2-1], and expanded on by the authors previously [27]. A number of bandlimited m-sequences from a given codeset produce an m-ary orthogonal signaling scheme (M-OCK). The auto- and cross-correlation properties of two such codesets for orders of $K = 11$ and $K = 13$ can be seen in Fig. 7 and Fig. 8.

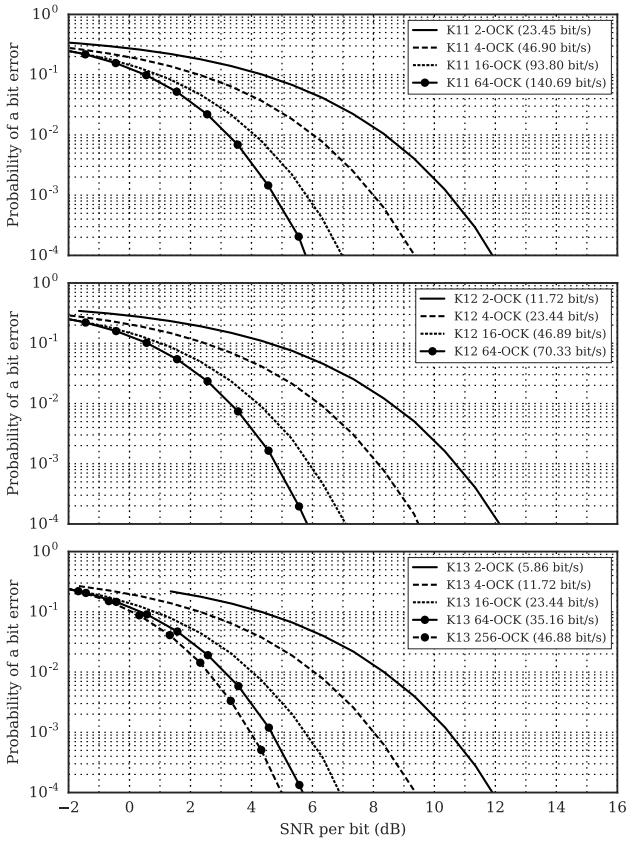

FIGURE 9. BER vs ϵ_b/N_0 for various values of M and K for M-ary orthogonal code keying. spreading bandwidth, B, of 8 kHz and F_s of 48 kHz. Direct comparisons can be made with the theoretical upper bounds of orthogonal signaling.

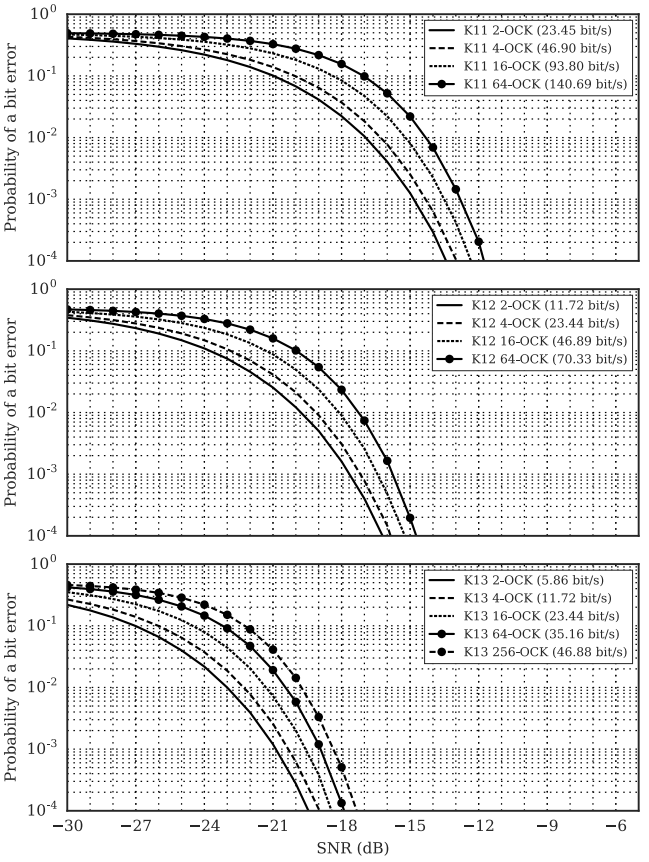

FIGURE 10. BER vs SNR for various values of M and K for M-ary orthogonal code keying. spreading bandwidth, B, of 8 kHz and F_s of 48 kHz. Process gains due to symbol duration and bandwidth are also evident here.

The performance of such a modulation scheme in an AWGN channel with a maximum-likelihood detector can be simulated for a range of orders, K, and modulations depths, M. For a sample frequency, F_s, of 48 kHz and bandwidth, B, of 8 kHz this can be seen in Fig. 9 and Fig. 10.

Fig. 9 shows that for a range of orders, K, and modulation depths, M, simulated performance is in line with the theoretical upper bounds of a M-ary orthogonal signaling scheme in Fig. 5.

Fig. 10 shows that for a given order, K, as the modulation depth, M, and data rate is increased there is no significant increase in symbol error.

III. RECEIVER DESIGN

Section II considers the detection of data symbols with frame synchronisation assumed. This section now describes the packet format and receiver structure including frame synchronisation.

A. FRAME SYNCHRONISATION

Like many acoustic modem designs, frame synchronisation is achieved by including a unique waveform (header) at the start of each data packet which the receiver correlates for. To operate at very low received-SNR, a high processing gain is required and reliable thresholding becomes particularly challenging. Processing gain is dependent on the bandwidth-time product of the header waveform. A longer duration waveform, for a given bandwidth, therefore has a greater spreading gain. Using a single longer PN symbol for the synchronisation header is a possible approach, however the Doppler intolerance of longer PN sequences and short channel coherence times would lead to a mismatch in correlation. Another approach is to use a number of shorter, unique PN sequences and combine their energy in such a way that more channel variation and Doppler can be tolerated. Example PN sequences, their combinations, and relative durations are shown in Fig. 11 where K represents the order of m-sequence used.

The receiver structure to detect a single PN sequence can be seen in Fig. 12. The signal is bandpass filtered and correlated with the stored PN sequence. The envelope is then normalised and threshold detection is used to detect the start of a packet.

The correlation and normalisation process can be expressed in (5) where h is the code, y is the input signal, L is the length of the code, and μ is the mean of the input signal, y.

$$c(t) = \frac{\sum_{n=0}^{L-1} h[n]\, y[n+t]}{\sqrt{\frac{1}{L}\sum_{n=0}^{L-1} (y[n]-\mu)^2}} \tag{5}$$

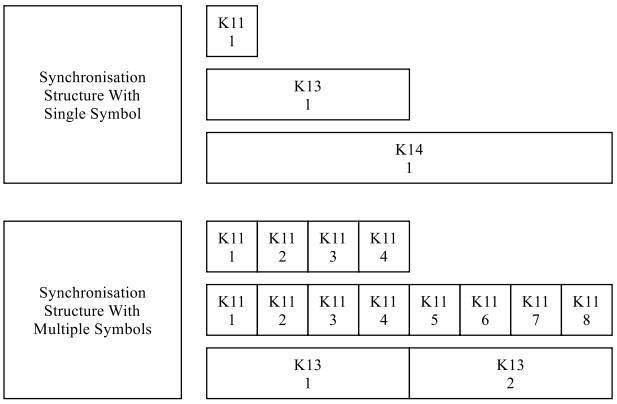

FIGURE 11. Synchronisation signal structures with a single PN Sequence or with multiple PN sequences. Showing the relative duration of each order of PN sequence. 1of K11, 1of K13 and 1of K14 for single symbol structures. 4of K11, 8of K11 and 2of K13 multiple symbol structures.

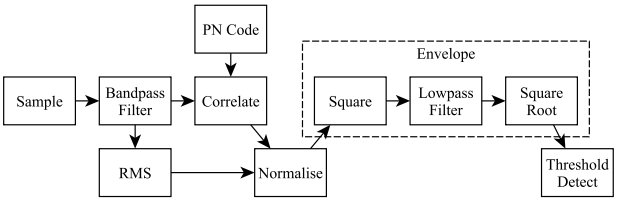

FIGURE 12. Receiver structure block design: synchronisation. Single code, correlation, normalisation, threshold detection.

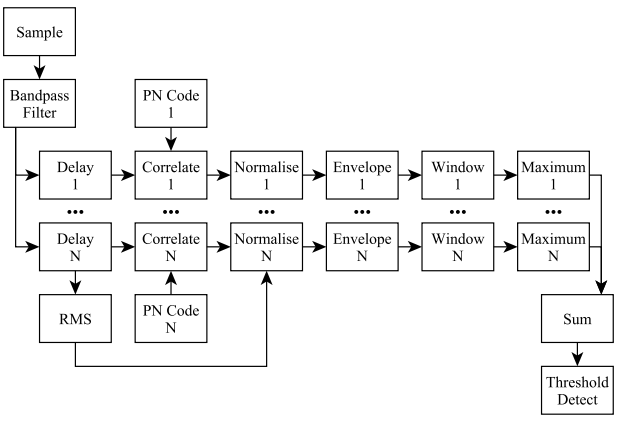

FIGURE 13. Receiver structure block design: synchronisation. Multiple codes, correlation, normalisation, summed threshold detection.

The receiver structure can then be extended to accommodate signals consisting of multiple unique PN sequences as shown in Fig. 13. Here the enveloped outputs of the correlators are windowed and the peak energy of each is combined before threshold detection is applied.

Synchronisation signal structures shown previously in Fig. 11 were constructed with a sample frequency, F_s, of 48 kHz and bandlimited between 8 kHz to 16 kHz. An AWGN channel was simulated to produce the synchronisation performance results shown in Fig. 14.

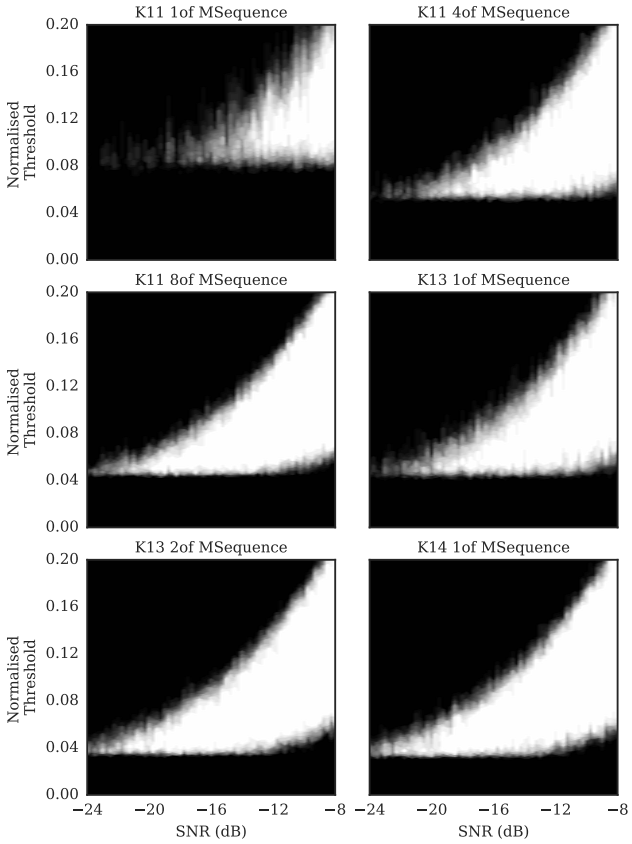

FIGURE 14. Synchronisation Performance Envelopes in AWGN Channel. For single sequence synchronisation structures, and multiple sequence structures. 1 of K11, 4 of K11, 8 of K11, 1 of K13, 2 of K13, and 1 of K14.

The envelope shows the bounding normalised threshold level and SNR values within which the receiver structure will successfully synchronise. Decreasing the normalised threshold value below this bound will result in false-positive detections. Combining the energy of the correlators for multiple sequences produces a visually similar performance to using a single symbol of equivalent total processing gain (bandwidth and duration). For example, 1of K14 with 2of K13 and 8of K11 have similar envelopes; as do 1of K13 and 4of K11. In simulation this approach appears equivalent, but the results from experiments with real underwater channels demonstrate the advantage of this approach in later sections of this paper.

The optimal threshold value to set is a trade-off between targeting low received-SNR and reducing the rate of false-positive detection. With long packet durations, false-positive detections are very problematic as they effectively lock out the receiver for the duration of an expected packet. During which time, there may have been a genuine arrival that the receiver is now unable to process.

B. DATA DEMODULATION

The data is demodulated using a bank of correlators and maximum likelihood decoder for each symbol. Time-windowing is used when comparing the correlator values to reduce

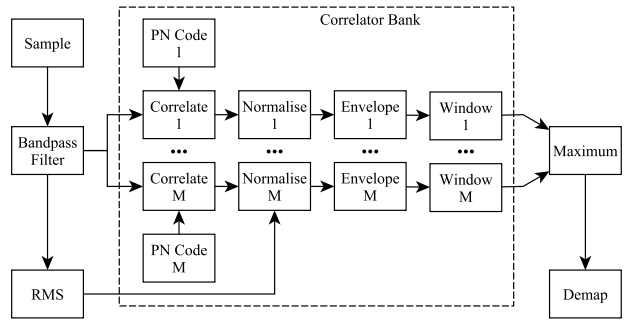

FIGURE 15. Receiver structure block design: data demodulation. Correlation, normalisation, envelope, windowing (12 samples), maximum value selection, demapping.

TABLE 1. Packet structure: data.

Structure	FEC	Data rate (bit/s)	Total data bits
100 of K11 64-OCK Symbols	Uncoded	140.69	600
100 of K11 64-OCK Symbols	RS 0.76 coderate 2 blocks of $[50, 38, 13]_{64}$–code	106.92	456
25 of K13 256-OCK Symbols	Uncoded	46.88	200
25 of K13 256-OCK Symbols	RS 0.76 coderate 1 block of $[25, 19, 7]_{256}$–code	35.63	152

inter-symbol interference, the width of the window being $2/B$. The position of the correlator peak value within the window is used to adjust symbol synchronisation throughout the packet. The windowing approach also greatly reduces computational load as only a small number of correlation coefficients (in this case 12) need to be computed per symbol for each code in the bank. The receiver structure for data demodulation can be seen in Fig. 15.

The packet structures used in simulation are shown in Table 1. Performance of both K11 64-OCK and K13 256-OCK data symbols were compared with and without Reed-Solomon error correction codes. The packets were repeatedly combined with varying levels of AWGN and demodulated; the results are shown in Fig. 16.

C. EXPERIMENTAL VALIDATION

To investigate the performance of synchronisation structures in experimental conditions a number of sequences are used. These structures allow a number of combinations of multiple symbols to be compared in the experiments. In this case 1of, 2of, 4of and 8of K11; and 1of, 2of and 4of K13 symbols.

All of the data packets described previously in Table 1 were incorporated into a single transmit audio file along with unique synchronisation headers for each payload. For experimental purposes, LFM chirps were also incorporated

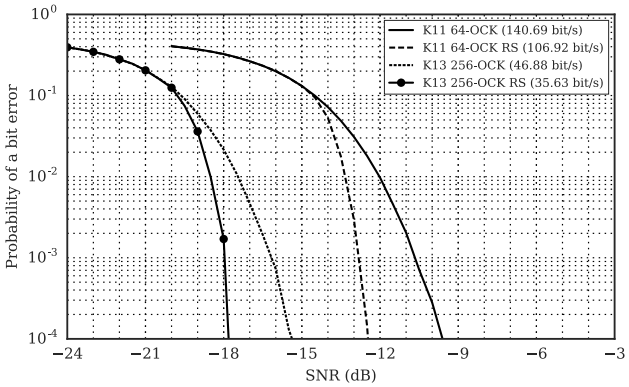

FIGURE 16. Receiver structure: data demodulation simulations. BER vs SNR for M-ary orthogonal code keying packets with the receiver structure. Spreading bandwidth, B, of 8 kHz and F_S of 48 kHz. Showing performance of K11 64-OCK (140.69 bit/s) and K13 256-OCK (46.88 bit/s). The performance using Reed-Solomon error correction codes is also shown for direct comparison. K11 64-OCK RS (106.92 bit/s) and K13 256-OCK RS (35.63 bit/s).

at 10dB higher power level than the M-OCK signals. In combination with silent periods, these chirps allow the received-SNR to be estimated at regular points during the recordings and also provided an audible confirmation that the signal was being received.

- Location: North Sea off Blyth, Northumberland
- Transmitter: Laptop playing audio. Power amplifier such that PN signal is limited to a source level of $<$170.8dB re 1μPa @ 1m or 1W of acoustic power. Transducer in water at depth of 30m.
- Receiver: Laptop recording audio. Bandpass filter and amplifier. Hydrophone in water at depth of 10m. Multiple 4 minute recordings taken at each range.
- Weather and Sea State: Clear skies. Calm sea.
- Geology: Rock shelf, areas covered with sediment, others exposed. Depth around 40m.
- Ranges: 100m, 500m, 1km, 2km, 5km and 10km.

Received-SNR estimates of the PN signals throughout the recordings were based on the 10dB offset from the LFM chirps (up and down) between packets along with the silence periods that preceded them. These can be seen in Fig. 17. At each range the received-SNR is seen to be relatively stable and steady throughout the four minute recording. The third recording at 5km shows a gradual decrease in received-SNR over the last two minutes. The 10km recordings show steady readings with occasional dips in received-SNR.

Channel impulse responses based on packets provide an indication of the multipath and rapidly changing channel conditions at each range as shown in Fig. 18 and Fig. 19. The channel impulse responses show the multipath reverberation and changing channel over the duration of a data packet (4.3 s) for each of the ranges under test. There are visibly strong multipath arrivals in the first 5 ms for all apart from 10km recordings. Paths are also seen to fade in and out during a packet duration, seen clearly in the recording at 2km.

The threshold values used for the varying synchronisation signal structures are shown in Table 2. The results of

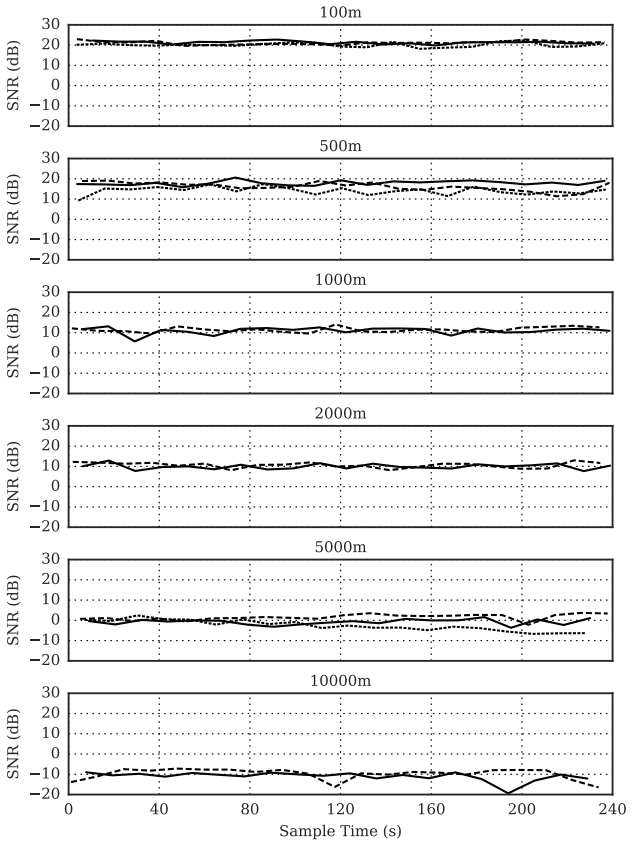

FIGURE 17. Sea trials SNR estimates with multiple recordings at each range.

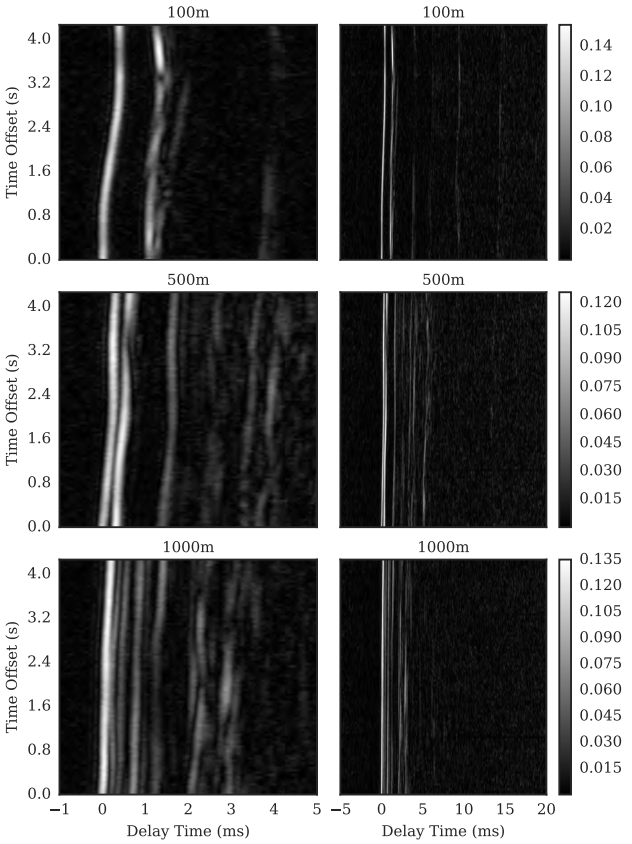

FIGURE 18. Sea trials channel impulse responses: 100m, 500m and 1km.

synchronisation counts for varying synchronisation signal structures are presented in Table 3. The duration of the entire transmit waveform is 23.273 s. Therefore a single four minute recording contains 10.3 repetitions of the relevant packets and synchronisation signal structures, which equates to 10 or 11 result points per recording. For ranges with three recordings, a synchronisation count of between 30 and 33 is expected; for two recordings, 20 to 22 synchronisation counts are expected.

In Table 3 the expected values are seen for all synchronisation signal structures for all ranges except 10km. Although, for 1of K11 there does appear to be the possibility of false positive detections. At 10km where the received-SNR reaches levels around −10dB there is a clear gradient in performance as the number of K11 symbols used increases. This shows that combining the energy of shorter symbols can produce equivalent results to using single symbols of the same duration/processing gain (1of K13) in a real underwater channel with multipath and changing conditions.

The data demodulation results for each recording are collated by range to produce performance points of bit error rate (BER) and packet success rate (PSR). These are tabulated in Table 4 for K11 64-OCK and Table 5 for K13 256-OCK.

The uncoded packets for K11 64-OCK and K13 256-OCK show bit errors at all ranges, however there are still significant packet success rates for K13 256-OCK across all ranges;

TABLE 2. Sea trials results: synchronisation thresholds.

	K11 Symbols				K13 Symbols		
	1 of	2 of	4 of	8 of	1 of	2 of	4 of
Threshold Value	0.12	0.10	0.08	0.07	0.07	0.06	0.05

TABLE 3. Sea trials results: synchronisation counts.

	Synchronisation Counts							
		K11 Symbols				K13 Symbols		
Range (m)	Expected	1 of	2 of	4 of	8 of	1 of	2 of	4 of
100	30–33	34	32	33	32	30	30	31
500	30–33	33	31	33	31	32	32	32
1000	20–22	22	21	22	21	21	21	21
2000	20–22	23	20	20	20	22	22	21
5000	30–33	32	31	31	31	30	30	30
10000	20–22	10	15	19	20	20	20	21

and for K11 64-OCK up to 5km. Reed-Solomon (RS) error correction coding is able to take the packet success rate up to 100% for K13 256-OCK RS across all ranges; and

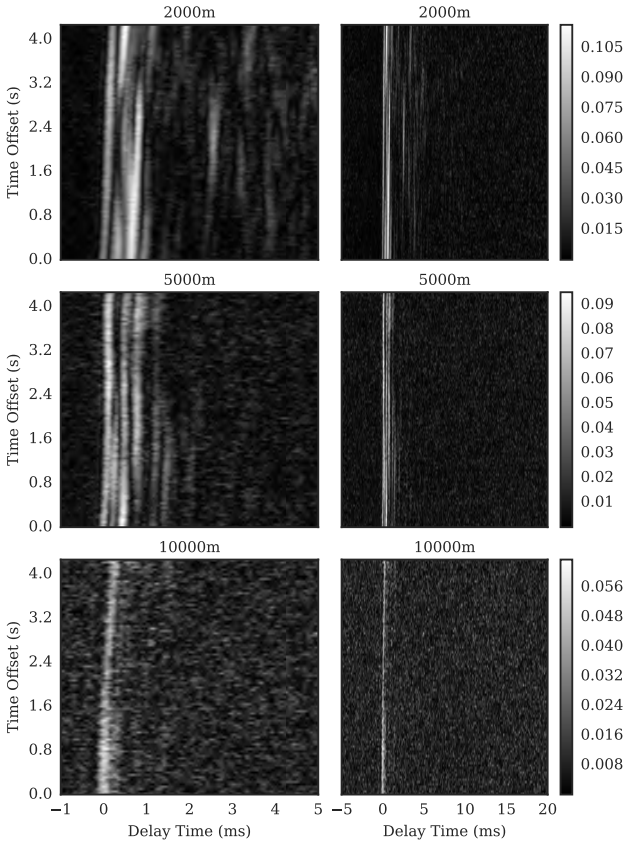

FIGURE 19. Sea trials channel impulse responses: 2km, 5km and 10km.

TABLE 4. Sea trials results: K11 64-OCK.

	Uncoded (140.69 bit/s)		RS (106.92 bit/s)	
Range (m)	BER	PSR	BER	PSR
100	3.056×10^{-4}	0.933	0.000	1.000
500	4.098×10^{-4}	0.918	0.000	1.000
1000	1.200×10^{-2}	0.975	0.000	1.000
2000	3.252×10^{-4}	0.951	0.000	1.000
5000	9.111×10^{-3}	0.850	5.263×10^{-3}	0.933
10000	5.841×10^{-2}	0.024	3.366×10^{-2}	0.550

K11 64-OCK RS up to 2km. However, RS also improves K11 64-OCK from 0.024 to 0.550 packet success rate at 10km.

These results show that both modulation schemes were able to be successfully received across a range of 5km transmitted with less than 1W of acoustic power and the K13 256-OCK continued to be reliable to 10km.

The channel recordings, although important to show the potential of the modulation schemes, did not have sufficiently low SNR to fully demonstrate the boundaries of performance and the time variability of SNR also complicates the analysis.

In order to investigate the SNR performance boundaries of the modulation schemes and receiver structures when

TABLE 5. Sea trials results: K13 256-OCK.

	Uncoded (46.88 bit/s)		RS (35.63 bit/s)	
Range (m)	BER	PSR	BER	PSR
100	4.098×10^{-4}	0.984	0.000	1.000
500	0.000	1.000	0.000	1.000
1000	0.000	1.000	0.000	1.000
2000	0.000	1.000	0.000	1.000
5000	1.967×10^{-3}	0.967	0.000	1.000
10000	9.756×10^{-4}	0.951	0.000	1.000

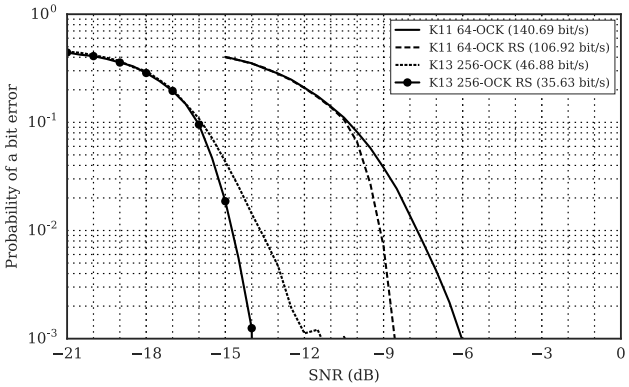

FIGURE 20. Receiver structure: data demodulation channel recording with AWGN. BER vs SNR for M-ary orthogonal code keying packets with the receiver structure. Channel recording for 100m (incorporating multipath and doppler effects) is combined with AWGN at various levels of SNR and processed with the receiver structure. Spreading bandwidth, B, of 8 kHz and F_s of 48 kHz. Showing performance of K11 64-OCK (140.69 bit/s) and K13 256-OCK (46.88 bit/s). The performance using Reed-Solomon error correction codes is also shown for direct comparison. K11 64-OCK RS (106.92 bit/s) and K13 256-OCK RS (35.63 bit/s).

the signals are subjected to real multipath channel effects, a subsection of the recording for 100m (with very high SNR) is combined with varying levels of simulated AWGN and processed with the receiver structure to produce performance curves as shown in Fig. 20.

The AWGN combined with the channel recording at 100m shows that performance limits for BER of 10^{-3} are -6dB for K11 64-OCK; -8.5dB for K11 64-OCK RS; -12dB for K13 256-OCK; and -14dB for K13 256-OCK RS.

It is important to note that the received-SNR estimates are based on the total received signal energy during the duration of a LFM chirp symbol. Given the long duration of the chirp (0.341 s) and the many multipath arrivals within the first 5 ms this means the SNR estimate is based on the total received energy of multiple paths. However the current receiver algorithm only utilises the first of these paths. In the case of the results presented in Fig. 20, the 100m channel has a signal-to-multipath ratio of approximately 4.4dB, meaning the effective SNR shown in the figure and the performance limits stated above are effectively 4.4dB lower. Expanding the receiver to

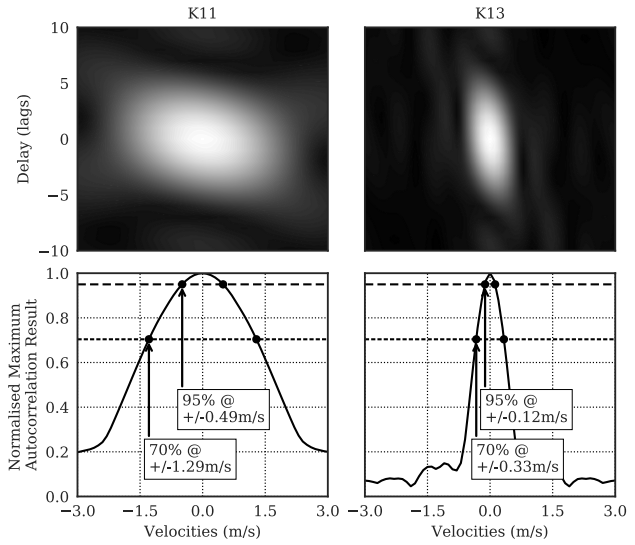

FIGURE 21. Ambiguity functions of K11 and K13 Symbols. Cross section figures show peak autocorrelation values at a range of velocities. For $c = 1500$m/s, $F_S = 48$ kHz and $B = 8$ kHz with K11 (42.65 ms) and K13 (170.65 ms). K11 autocorrelation reaches 95% at ±0.49m/s, and 70% at ±1.29m/s. K13 autocorrelation reaches 95% at ±0.12m/s, and 70% at ±0.33m/s.

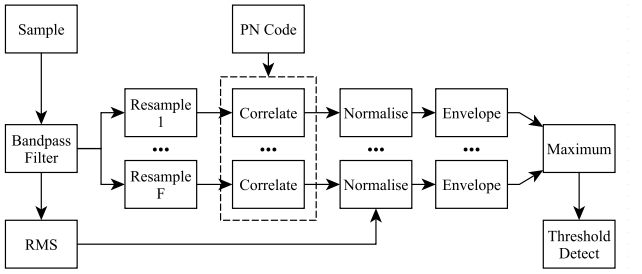

FIGURE 22. Receiver structure block design: synchronisation. Single code, resampling, correlation, normalisation, envelope, maximum threshold detection.

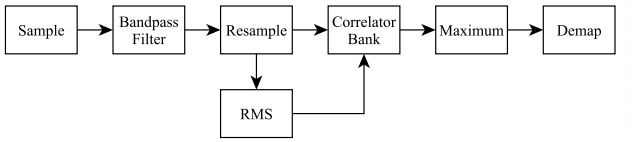

FIGURE 23. Receiver structure block design: data demodulation. Resampling, correlation, normalisation, envelope, maximum value selection, demapping.

coherently combine a number of these paths, via a RAKE-like structure, should deliver performance which closely matches the simulation results.

IV. DOPPLER COMPENSATION

The ambiguity function plots of the two PN sequences used throughout this research, K11 and K13 symbols, are shown in Fig. 21.

Where the ambiguity function, $A(\delta f, \delta t)$, is given by [28, 29, eq. (6)]. Where $s(f_0, \tau)$ is the nominal time-domain signal with carrier frequency f_0, $s(f_0 + \delta f, \tau - \delta t)$ is the signal shifted in time by δt and in frequency by the Doppler shift δf.

$$A(\delta f, \delta t) = \left| \int_{-\infty}^{\infty} s(f_0, \tau) * (f_0 + \delta f, \tau - \delta t)\, d\tau \right|^2 \quad (6)$$

The longer duration symbols, K13, suffer the greatest mismatch with Doppler shift, with the autocorrelation peak value falling away to 70% with a relative velocity of only ±0.33m/s. Even with the shorter symbol duration of K11 the drop to 70% occurs after ±1.29m/s. To put this into perspective, the velocity of typical AUVs can be in the range of 0m/s to 2.5m/s. Consequently the receiver design will require compensation for Doppler effects in those applications with non-stationary platforms.

Techniques for Doppler compensation with PN sequences have been covered before by Johnson *et al.* [30], and also referred to by Sharif *et al.* [31]. Here, a bank of correlators is loaded with Doppler shifted versions of the sequence across a range of Doppler shifts. The input signal is correlated across the entire bank and the maximum correlator value is then used to test for synchronisation and to estimate the starting Doppler shift of the signal.

It is possible to use the Doppler compensation technique by Johnson *et al.* [30] mentioned previously, but with the key difference of loading each correlator in the bank with the same PN sequence, and instead resampling the input signal to each correlator to potentially remove the frequency shift due to Doppler effect. Resampling is performed in the method shown by Sharif *et al.* [31].

A. SYNCHRONISATION

Taking the receiver structure for synchronisation in Fig. 12 the block design is extended to incorporate the resamplers and correlator bank as shown in Fig. 22. The number and distribution of the resamplers and correlators is dependent on the ambiguity functions shown previously. To cover a suitable range, of say ±2.7m/s, with minimum ripple in correlator peak value of 95%, this would give 25 resampler streams spaced at 0.225m/s steps for a K13 symbol. The synchronisation structure, as well as searching for the synchronisation header across a range of Doppler shifts, will also provide the starting Doppler estimate for the data packet demodulation.

B. DATA DEMODULATION

The simplest Doppler compensation that can be applied here is to take the receiver structure from Fig. 15 and prepend a single resampler stage which is set to the Doppler estimate determined by the synchronisation structure. This so called 'static' resampling receiver structure is shown in Fig. 23.

To operate with longer duration packets and platform acceleration (non-uniform Doppler shift), it is possible to expand the synchronisation structure to track changes in Doppler shift on a symbol-by-symbol basis in the data packet.

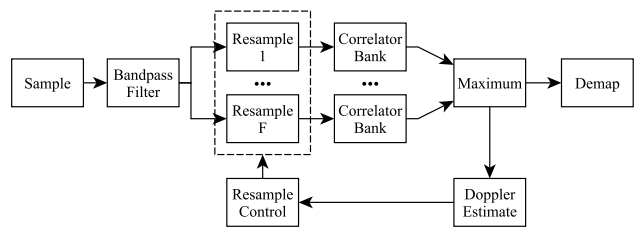

FIGURE 24. Receiver structure block design: data demodulation. Resampling, correlation, normalisation, maximum value selection, tracking, demapping.

This tracking resampler structure is shown in Fig. 24. The distribution of resampler values is 7 streams targeting a 95% ripple, so for K11 symbols this is a range of ±2.7m/s in steps of 0.9m/s. For the K13 symbols this is a range of ±0.675m/s in steps of 0.225m/s.

However, the absolute resampler values of the seven streams are relative to the value used in the 'centre' stream. This centre stream value is initially set to the Doppler estimate produced by the synchronisation receiver structure. As the receiver processes the received signal symbol-by-symbol, the centre resampler value is adjusted and results in the absolute resampler values of the other size streams also shifting accordingly. This allows the receiver to cover a much larger overall range of Doppler shift throughout the duration of the whole packet, but on a symbol-by-symbol basis provides fine resolution refinement. The full range of the resamplers sets the maximum acceleration that can be accommodated by the receiver structure.

For example, for the K11 symbols if the initial Doppler estimate is 1.0m/s then the absolute resampler values will cover the range of −1.7m/s to 3.7m/s.

C. EXPERIMENTAL VALIDATION

An aerial view of the Royal Quays Marina, North Shields can be seen in Fig. 25. This shows the location of the receiver and the paths, A, B and C, that were taken by the motorboat towing the transmitter.

- Location: Royal Quays Marina, North Shields
- Transmitter: Motor boat platform in motion. Laptop playing audio. Acoustic power amplifier. Weighted transducer in water at depth of 2m.
- Receiver: Laptop recording audio. Bandpass filter and amplifier. Hydrophone in water at depth of 5m. Multiple 4 minute recordings taken for each motion type.
- Weather and Water State: Clear skies. Calm water.
- Geology: Stone wall marina with floating pontoons. Depth around 10m.
- Motion Types: Constant 1.11m/s along Path A, Constant 2.22m/s along Path A, Varying 0m/s to 2.22m/s along Path A, Perpendicular Constant 2.22m/s along Path B and Path C.

Fig. 26 shows the channel impulse responses for each motion type. For all recordings there are strong multipath

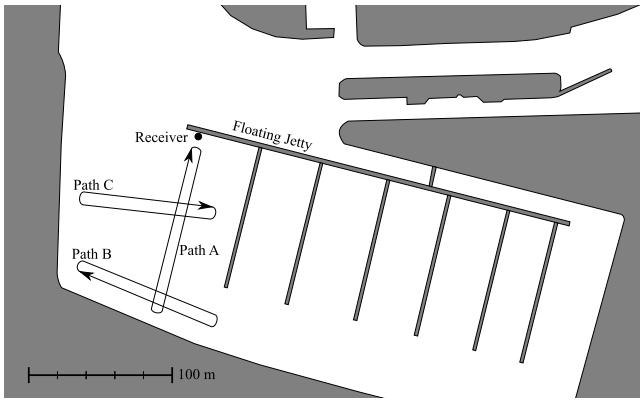

FIGURE 25. Marina aerial view.

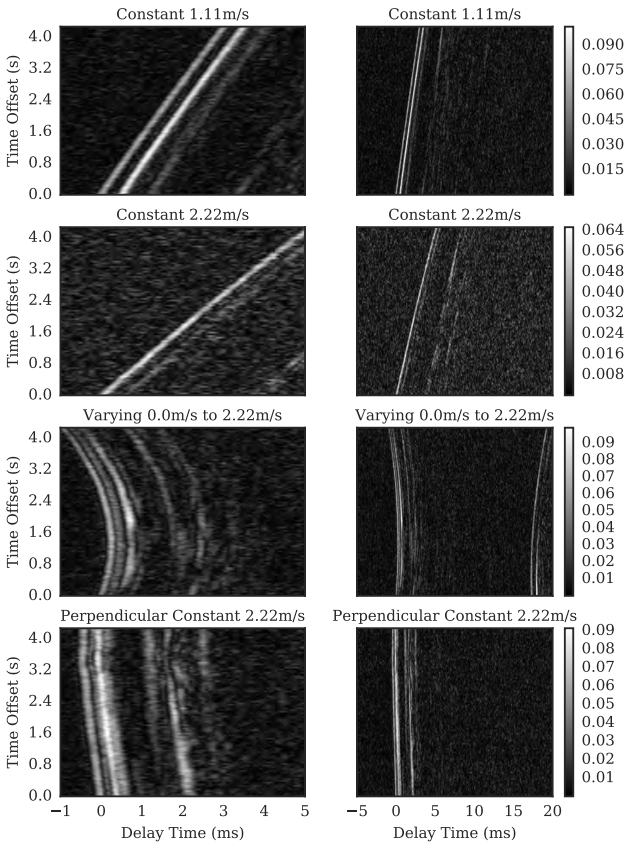

FIGURE 26. Marina channel impulse responses.

arrivals, sometimes up to 20 ms after the first arrival. The stone walls of the marina provide strong acoustic reflectors. The channel changes over the duration of a data packet (4.3 s) are more pronounced than in the sea trials previously. Again, the multipath arrivals show fading in and out through the packet duration. In the Varying 0m/s to 2.22m/s impulse response it is possible to see that the later arrivals, after 15 ms, show a mirror image shift to the first arrivals. This is an important factor in any future receiver structure that combines energy from multiple paths - each path has an independent

TABLE 6. Marina trials results: synchronisation counts.

	Synchronisation Counts							
		K11 Symbols				K13 Symbols		
Motion Type	Expected	1 of	2 of	4 of	8 of	1 of	2 of	4 of
Constant 1.11m/s	40–44	42	41	40	40	8	9	11
Constant 2.22m/s	40–44	16	21	27	31	0	0	1
Varying 0.0m/s to 2.22m/s	30–33	29	28	30	29	1	1	2
Perpendicular Constant 2.22m/s	40–44	43	40	41	41	24	26	31

TABLE 7. Marina trials results: synchronisation counts with doppler compensation.

		Synchronisation Counts	
Doppler Compensation		None	Fine Search
		K13 Symbols	K13 Symbols
Motion Type	Expected	1 of	1 of
Constant 1.11m/s	164–168	26	168
Constant 2.22m/s	164–168	12	165
Varying 0.0m/s to 2.22m/s	123–126	15	126
Perpendicular Constant 2.22m/s	164–168	81	165

Doppler shift to take account of, and to track throughout the packet duration.

The synchronisation counts for varying synchronisation signal structures are presented in Table 6. The results for each recording have been collated by motion type. The sea trials results in the previous section showed the effect of SNR, here with high SNR readings the effect of Doppler is the dominant factor on performance. As before, the duration of the entire transmit waveform is 23.273 s. Therefore a single four minute recording contains 10.3 repetitions of the relevant packets and synchronisation signal structures, which equates to 10 or 11 result points per recording. For motion types with four recordings, a synchronisation count of between 40 and 44 is expected; for three recordings, 30 to 33 synchronisation counts are expected. For the lower speed of Constant 1.11m/s the K11 symbol structures synchronise successfully, whereas for the K13 symbol structures the synchronisation counts are greatly reduced. As the speed is increased to 2.22m/s the K13 symbol structures drop to almost total failure to synchronise. The K11 symbols show a gradient increasing as more symbols are combined which is consistent with the ambiguity plots in Fig. 21 which show that as the velocity reaches 2.22m/s the correlation peak drops to 50%.

The varying and perpendicular motion types contain periods of low speed, and hence low Doppler effect, so both K11 and K13 symbol structures have successful synchronisation counts for part of this period.

In general, both symbol types K11 and K13, even when used in multiple symbol structures, suffer synchronisation failures from Doppler beyond certain speeds. However, for K11 symbols this velocity is much higher than K13 before it fails to synchronise. In conjunction with the sea trial results in the previous section this may be a suitable technique to create a signal structure with inbuilt Doppler tolerance whilst retaining total processing gain due to signal spreading over long durations.

The performance of the Doppler compensation receiver structure in Fig. 22 was investigated in the same channel with significant Doppler shift using resampling parameters that cover a range of ± 2.7m/s in steps of 0.225m/s resulting in a total of 25 streams.

The successful synchronisation counts are shown in Table 7. A single four minute recording contains 10.3 repetitions of the four relevant packets and synchronisation signal structures, which equates to 41 or 42 result points per recording. For ranges with four recordings, a synchronisation count of between 164 and 168 is expected; for three recordings, 123 to 126 synchronisation counts are expected.

The results in Table 7 show a clear improvement when Doppler compensation is utilised across the four motion types. These results show that the receiver structure and signal resamplers are a viable solution to compensating for Doppler effects on the transmitted signal.

Collated results for all of the Marina Trials recordings have been tabulated in Table 8 for K11 64-OCK and K11 64-OCK RS; and in Table 9 for K13 256-OCK and K13 256-OCK RS.

These results show that any Doppler compensation in the receiver structure has a positive effect when compared to the uncompensated signals for both K11 64-OCK and K13 256-OCK modulation schemes. Although there is little difference in performance for K11 64-OCK between static and tracking resampler compensation, for K13 256-OCK there is an improvement in performance with the tracking resampler showing improvement over the static resampler.

The performance for recording "motion08 - Constant 2.22m/s" is shown in Fig. 27 for No Doppler Compensation; Static Resampler Doppler Compensation; and Tracking Resampler Doppler Compensation. The results are tabulated in Table 10 for K11 64-OCK and K11 64-OCK RS; and in Table 11 for K13 256-OCK and K13 256-OCK RS.

Fig. 27 shows the correlation between the received-SNR and the velocities, where the peak SNR values occur as the

TABLE 8. Marina trials recording results: K11 64-OCK - all recordings.

	K11 64-OCK Uncoded		K11 64-OCK RS	
Doppler Compensation	BER	PSR	BER	PSR
None	3.205×10^{-1}	0.197	3.118×10^{-1}	0.211
Static Resampler	3.213×10^{-2}	0.704	2.458×10^{-2}	0.836
Tracking Resampler	3.548×10^{-2}	0.714	2.751×10^{-2}	0.822

TABLE 9. Marina trials recording results: K13 256-OCK - all recordings.

	K13 256-OCK Uncoded		K13 256-OCK RS	
Doppler Compensation	BER	PSR	BER	PSR
None	4.256×10^{-1}	0.095	4.286×10^{-1}	0.110
Static Resampler	4.757×10^{-2}	0.744	3.426×10^{-2}	0.844
Tracking Resampler	2.425×10^{-2}	0.875	2.589×10^{-2}	0.890

boat draws near the receiver platform, and the velocity crosses zero as the boat makes the turn along Path A. The relative velocities experienced based on the Doppler estimates show the steady 2.22m/s at the peaks and troughs with rapid acceleration/deceleration as the boat makes the turn. In this recording, with no Doppler compensation all packets fail apart from a single K11 64-OCK packet which occurs as the velocity crosses 0m/s. With the use of the static resampler Doppler compensation a distinct improvement can be seen in packet successes for the durations where the velocity is constant. However, the period of rapid acceleration/deceleration shows failed packets.

It can also be seen that with tracking Doppler compensation the number of failed packets is again reduced. Table 10 shows the packet success rate total for K11 64-OCK remains almost the same for static to tracking Doppler compensation. Table 11 shows that there is an improvement in K13 256-OCK performance from static to tracking Doppler compensation with only a single failed packet remaining. The importance of accurate Doppler compensation is again emphasised for the large BT product waveforms.

V. DISCUSSION

Experimental validation in sea trials shows successful synchronisation and a high proportion of error-free packets received at 10km with a signal transmit power limited to $<$170.8dB re 1μPa @ 1m or 1W of acoustic power. Successful packets were received at this range for K11 64-OCK, K11 64-OCK RS, K13 256-OCK, and K13 256-OCK RS.

Sea trial recordings with SNR adjusted by adding additional AWGN show successful data demodulation with BER

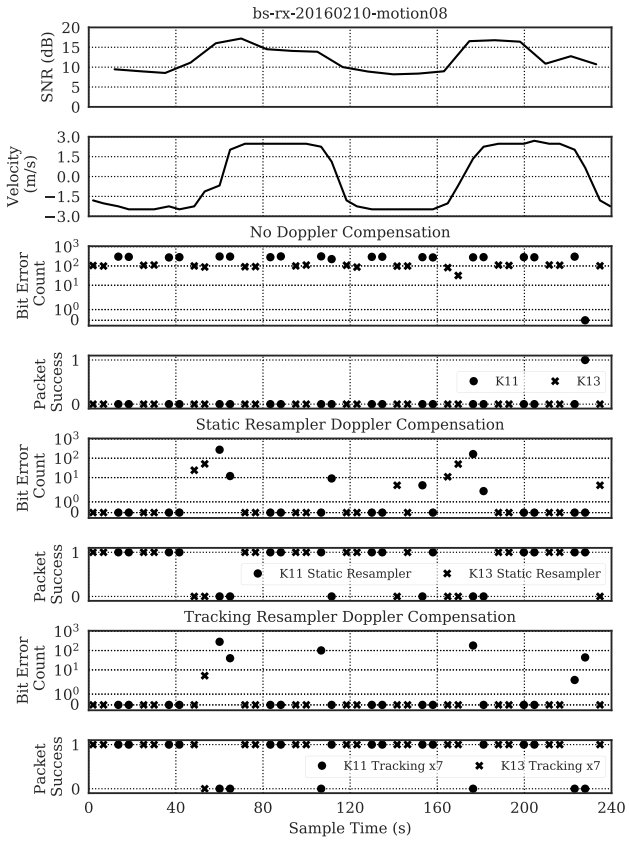

FIGURE 27. Marina trials recording results - motion08 recording. Showing performance of K11 64-OCK (140.69 bit/s) and K13 256-OCK (46.88 bit/s). With no doppler compensation, static resampler doppler compensation, and tracking resampler doppler compensation.

TABLE 10. Marina trials recording results: K11 64-OCK - motion08 recording.

	K11 64-OCK Uncoded		K11 64-OCK RS	
Doppler Compensation	BER	PSR	BER	PSR
None	4.572×10^{-1}	0.050	4.886×10^{-1}	0.000
Static Resampler	3.883×10^{-2}	0.700	7.237×10^{-2}	0.800
Tracking Resampler	5.433×10^{-2}	0.700	8.750×10^{-2}	0.700

of 10^{-3} down to $-$14dB of the K13 256-OCK RS at a data rate of 35.63 bit/s. Given packet sizes of 200 bits this BER would equate to a large proportion of error-free packets. Channel capacity according to Shannon-Hartley for this SNR and bandwidth is 450.57 bit/s resulting in a channel capacity utilisation of 7.91%.

The K11 64-OCK RS signal with a data rate of 106.92 bit/s shows BER of 10^{-3} at $-$8.5dB, with packet sizes of 600 bits again this would result in successful packets. Channel capacity at this SNR and bandwidth is 1524.96 bit/s resulting in a channel capacity utilisation of 7.01%.

TABLE 11. Marina trials recording results: K13 256-OCK - motion08 recording.

	K13 256-OCK Uncoded		K13 256-OCK RS	
Doppler Compensation	BER	PSR	BER	PSR
None	4.886×10^{-1}	0.000	5.006×10^{-1}	0.000
Static Resampler	3.429×10^{-2}	0.714	2.990×10^{-3}	0.909
Tracking Resampler	1.190×10^{-3}	0.952	0.000	1.000

The previously reported techniques using multiband OFDM [17], [18] had a channel capacity utilisation of 4.09% for the lower data rate of 4.2 bit/s at −17dB, and a channel capacity utilisation of 10.21% for the higher data rate of 78 bit/s at −8dB, both with a bandwidth of 3.6 kHz. The techniques using DSSS with turbo equalization [19] showed channel capacity utilisation rates of 2.03% and 7.35% for the lower and higher data rates at −14dB and −6.5dB respectively. The MCSS technique [15], [16] produced the highest channel capacity utilisation rate of 23.09% for 75 bit/s at −12dB.

With these SNR levels in mind, the 7.91% and 7.01% channel capacity utilisation by M-OCK signals and receivers falls well within the region of performance by the state-of-the-art techniques. However, since the current receiver structure does not combine the energy from multiple arrivals but only one path, the effective SNR in these experiments is substantially lower. Future development of the receiver to combine the energy from multipath arrivals is expected to push this utilisation to at least 20%.

Frame synchronisation using the multiple symbol header waveforms has been shown, in a real underwater acoustic channels with significant Doppler effects, to outperform single symbol header waveforms of the equivalent processing gain or BT product.

Data demodulation with significant Doppler effects has been shown to be successful when a static resampler receiver structure is used for constant velocity scenarios. However the tracking resampler receiver structure has been shown to be more successful where there is significant acceleration.

The studies by Kastelein *et al*. [4] showed that for a source level of 170dB re 1μPa @ 1m the modulated FSK signal produced an estimated discomfort zone radius of 1.26km. The modulated FSK signal spectrogram more closely resembled that of the M-OCK signal based on bandwidth spreading and message duration in these experiments.

Therefore, given that the same source level was used in the Sea Trials with successful communication at the 10km range, this would produce a receivable-discomfort ratio of 10:1.26 = 7.94. At this range the K13 256-OCK signals were still producing near 100% packet success rates, so this ratio could be further improved upon, particularly with enhanced error correction codes.

VI. CONCLUSION

The signal design and receiver structures proposed in this paper have achieved reliable communication at SNR as low as −14dB with channel capacity utilisation which compares favourably with previously published work. The ability to maintain reliable synchronisation in the presence of time varying Doppler effects has also been demonstrated. Advantages are demonstrated in terms of impact on marine life and the likely discomfort zone, as well as the implementation complexity when compared to state-of-the-art techniques. The scheme developed is a promising technique to minimise the impact of underwater communication networks on marine life.

With future work on optimum error correction coding as well as the coherent combination of multipath signal energy, the performance and channel capacity utilisation could be increased further.

ACKNOWLEDGMENT

The authors would like to thank the staff at Royal Quays Marina, North Shields; the staff and School of Marine Science and Technology for the use of the RV Princess Royal; and the SEA Lab team at Newcastle University.

REFERENCES

[1] W. J. Richardson, C. R. Greene, Jr., C. I. Malme, and D. H. Thomson, *Marine Mammals and Noise*. San Francisco, CA, USA: Academic, 1995.

[2] O. Commission, "Overview of the impacts of anthropogenic underwater sound in the marine environment," Tech. Rep. 441/2009, 2009, p. 134.

[3] K. Lucke, U. Siebert, P. A. Lepper, and M.-A. Blanchet, "Temporary shift in masked hearing thresholds in a harbor porpoise (phocoena phocoena) after exposure to seismic airgun stimuli," *J. Acoust. Soc. Amer.*, vol. 125, no. 6, pp. 4060–4070, 2009.

[4] R. Kastelein, W. Verboom, M. Muijsers, N. Jennings, and S. Van der Heul, "The influence of acoustic emissions for underwater data transmission on the behaviour of harbour porpoises (phocoena phocoena) in a floating pen," *Marine Environ. Res.*, vol. 59, no. 4, pp. 287–307, 2005. [Online]. Available: http://dx.doi.org/10.1016/j.marenvres.2004.05.005

[5] R. Kastelein, D. De Haan, N. Vaughan, C. Staal, and N. Schooneman, "The influence of three acoustic alarms on the behaviour of harbour porpoises (phocoena phocoena) in a floating pen," *Marine Environ. Res.*, vol. 52, no. 4, pp. 351–371, 2001.

[6] R. A. Kastelein, H. T. Rippe, N. Vaughan, N. M. Schooneman, W. C. Verboom, and D. De Haan, "The effects of acoustic alarms on the behavior of harbor porpoises (phocoena phocoena) in a floating pen," *Marine Mammal Sci.*, vol. 16, no. 1, pp. 46–64, 2000.

[7] T. Yang and W.-B. Yang, "Performance analysis of direct-sequence spread-spectrum underwater acoustic communications with low signal-to-noise-ratio input signals," *J. Acoust. Soc. Amer.*, vol. 123, no. 2, pp. 842–855, 2008. [Online]. Available: http://scitation.aip.org/content/asa/journal/jasa/123/2/10.1121/1.2828053

[8] J. Ling, H. He, J. Li, W. Roberts, and P. Stoica, "Covert underwater acoustic communications," *J. Acoust. Soc. Amer.*, vol. 128, no. 5, pp. 2898–2909, 2010. [Online]. Available: http://scitation.aip.org/content/asa/journal/jasa/128/5/10.1121/1.3493454

[9] J. Ling, H. He, J. Li, W. Roberts, and P. Stoica, "Covert underwater acoustic communications: Transceiver structures, waveform designs and associated performances," in *Proc. OCEANS*, Sep. 2010, pp. 1–10.

[10] L. Lei, F. Xu, Y. Xu, and Y. Wu, "A chaotic direct sequence spread spectrum communication system in shallow water," in *Proc. Int. Conf. Control, Autom. Syst. Eng. (CASE)*, 2011, pp. 1–4.

[11] T.-S. Ahn, J.-W. Jung, H.-H. Sung, D.-W. Lee, and T.-D. Park, "Turbo equalization for covert communication in underwater channel," in *Proc. 8th Int. Conf. Ubiquitous Future Netw. (ICUFN)*, 2016, pp. 462–464.
[12] W. Jans, I. Nissen, F. Gerdes, E. Sangfelt, C.-E. Solberg, and P. van Walree, *UUV-Covert Acoustic Communications Preliminary Results of the First Sea Experiment*. Neuilly-sur-Seine, France: NATO Res. Technol. Org., 2006.
[13] P. A. Van Walree, T. Jenserud, and M. Smedsrud, "A discrete-time channel simulator driven by measured scattering functions," *IEEE J. Sel. Areas Commun.*, vol. 26, no. 9, pp. 1628–1637, Dec. 2008.
[14] M. Palmese, G. Bertolotto, A. Pescetto, and A. Trucco, "Experimental validation of a chirp-based underwater acoustic communication method," in *Proc. Meetings Acoust.*, 2008, vol. 4. no. 1, p. 030002.
[15] P. Van Walree, E. Sangfelt, and G. Leus, "Multicarrier spread spectrum for covert acoustic communications," in *Proc. OCEANS*, 2008, pp. 1–8.
[16] P. A. van Walree and G. Leus, "Robust underwater telemetry with adaptive turbo multiband equalization," *IEEE J. Ocean. Eng.*, vol. 34, no. 4, pp. 645–655, Oct. 2009.
[17] G. Leus, P. van Walree, J. Boschma, C. Fanciullacci, H. Gerritsen, and P. Tusoni, "Covert underwater communications with multiband ofdm," in *Proc. OCEANS*, Sep. 2008, pp. 1–8.
[18] G. Leus and P. A. van Walree, "Multiband OFDM for covert acoustic communications," *IEEE J. Sel. Areas Commun.*, vol. 26, no. 9, pp. 1662–1673, Dec. 2008. [Online]. Available: http://ieeexplore.ieee.org/stamp/stamp.jsp?arnumber=4686805
[19] E. Sangfelt, B. Nilsson, and J. Israelsson, "Covert underwater communication experiments using dsss and turbo equalization," in *Proc. UDT Eur.*, 2008, pp. 1–18.
[20] P. van Walree *et al.*, "UUV covert acoustic communications," in *Proc. 3rd Conf. Underwater Acoustic Meas., Technol. Results*, 2009, p. 254.
[21] H. Dol and P. van Walree, "Underwater acoustic communication research at TNO—Past and present," in *Proc. IEEE-Spain OCEANS*, Jun. 2011, pp. 1–6.
[22] K. E. Dimitrov, J. A. Neasham, B. S. Sharif, C. C. Tsimenidis, and G. M. Goodfellow, "Low-power environmentally friendly underwater acoustic communication using pseudo-noise spreading sequences," in *Proc. Yeosu OCEANS*, May 2012, pp. 1–5. [Online]. Available: http://ieeexplore.ieee.org/stamp/stamp.jsp?arnumber=6263622
[23] J. G. Proakis and M. Salehi, *Digital Communications*. New York, NY, USA: McGraw-Hill, 2008. [Online]. Available: https://books.google.co.uk/books?id=ksh0GgAACAAJ
[24] L.-L. Yang and L. Hanzo, "A recursive algorithm for the error probability evaluation of M-QAM," *IEEE Commun. Lett.*, vol. 4, no. 10, pp. 304–306, Oct. 2000. [Online]. Available: http://ieeexplore.ieee.org/stamp/stamp.jsp?arnumber=880816
[25] S. W. Golomb, *Shift Register Sequences* (Holden-Day Series in Information Systems). San Francisco, CA, USA: Holden-Day, 1967. [Online]. Available: https://books.google.co.uk/books?id=3tpQAAAAMAAJ
[26] S. W. Golomb and G. Gong, *Signal Design for Good Correlation: For Wireless Communication, Cryptography, and Radar*. Cambridge, U.K.: Cambridge Univ. Press, 2005. [Online]. Available: https://books.google.co.uk/books?id=DhYXL4miZj4C
[27] B. Sherlock, C. C. Tsimenidis, and J. A. Neasham, "Signal and receiver design for low-power acoustic communications using m-ary orthogonal code keying," in *Proc. OCEANS-Genova*, May 2015, pp. 1–10.
[28] X. Lurton, *An Introduction to Underwater Acoustics: Principles and Applications*, 2nd ed. Berlin, Germany: Springer, 2010. [Online]. Available: https://books.google.co.uk/books?id=PFXgLQAACAAJ
[29] *Sonar Acoustics Handbook*. NURC, La Spezia, Italy. 2008, 2008.
[30] M. Johnson, L. Freitag, and M. Stojanovic, "Improved doppler tracking and correction for underwater acoustic communications," in *Proc. IEEE Int. Conf. Acoust., Speech, Signal Process. (ICASSP)*, vol. 1. Apr. 1997, pp. 575–578.
[31] B. S. Sharif, J. Neasham, O. R. Hinton, and A. E. Adams, "A computationally efficient Doppler compensation system for underwater acoustic communications," *IEEE J. Ocean. Eng.*, vol. 25, no. 1, pp. 52–61, Jan. 2000.

BENJAMIN SHERLOCK (M'17) received the M.Eng. degree in microelectronics and software engineering from Newcastle University, Newcastle upon Tyne, U.K., in 2003. He was a Consultant Engineer with the Electronics and Software Team, RCID, Newcastle University, until 2013. In 2013, he undertook a Ph.D. project in environmentally friendly underwater acoustic communications based on spread-spectrum techniques. He is currently a Research Associate with the School of Engineering, Newcastle University, focusing on underwater acoustic signal processing applications in wireless distributed sensor networks. He is a member of the IEEE Oceanic Engineering Society.

JEFFREY A. NEASHAM received the B.Eng. degree in electronic engineering from Newcastle University, Newcastle upon Tyne, U.K., in 1994. He was with Newcastle University until 2007 as a Research Associate on research and commercial product development in underwater acoustic communication, sonar imaging, and wireless sensor networks, before taking up an academic post. He is currently a Senior Lecturer in communications and signal processing with the School of Electrical and Electronic Engineering, Newcastle University. He has authored over 80 conference and journal publications and his work on underwater modem design has been commercialized by three U.K. companies. His research interests are in underwater acoustic signal processing and device design, wireless communication networks, and biomedical instrumentation.

CHARALAMPOS C. TSIMENIDIS (M'05–SM'12) received the Ph.D. degree in communications and signal processing from Newcastle University in 2002. He is a Senior Lecturer in signal processing for communications with the School of Electrical and Electronic Engineering. His main research expertise and interests is in the area of adaptive array receivers for wireless communications, including demodulation algorithms, network coding, and protocol design for radio frequency and underwater acoustic channels. During the last 13 years, he has authored over 175 conference and journal papers, supervised successfully three M.Phil. and 36 Ph.D. students and made contributions in the area of arrayed receiver design for doubly spread multipath fading channels to several European funded research projects, including Long Range Telemetry in Ultra-Shallow Channels (LOTUS) - EU Contract Number: MAS3-CT97-0099, Shallow Water Acoustic Network EU Contract Number: MAS3-CT97-0107, and Acoustic Communication Network for the Monitoring of the Underwater Environment in Coastal Areas (ACME) - EU Contract Number: EVK3-CT-2000-00039. He is a member of the IET. He has been involved regularly in Technical Program Committee for over 100 Symposia of esteemed International conferences. He has offered a Professional Tutorials at esteemed, IEEE-sponsored, International Conferences with title Waveform Design for Underwater Acoustic Communications.